One-step assay for detecting influenza virus using dynamic light scattering and gold nanoparticles

ARTICLE *in* THE ANALYST · JUNE 2011

Impact Factor: 4.11 · DOI: 10.1039/c1an15303j · Source: PubMed

4 AUTHORS, INCLUDING:

Cheryl A Jones
University of Georgia
13 PUBLICATIONS **219** CITATIONS
SEE PROFILE

Stephen Mark Tompkins
University of Georgia
84 PUBLICATIONS **2,014** CITATIONS
SEE PROFILE

Ralph Tripp
University of Georgia
214 PUBLICATIONS **10,442** CITATIONS
SEE PROFILE

Analyst

Interdisciplinary detection science

www.rsc.org/analyst

Volume 136 | Number 15 | 7 August 2011 | Pages 3025–3204

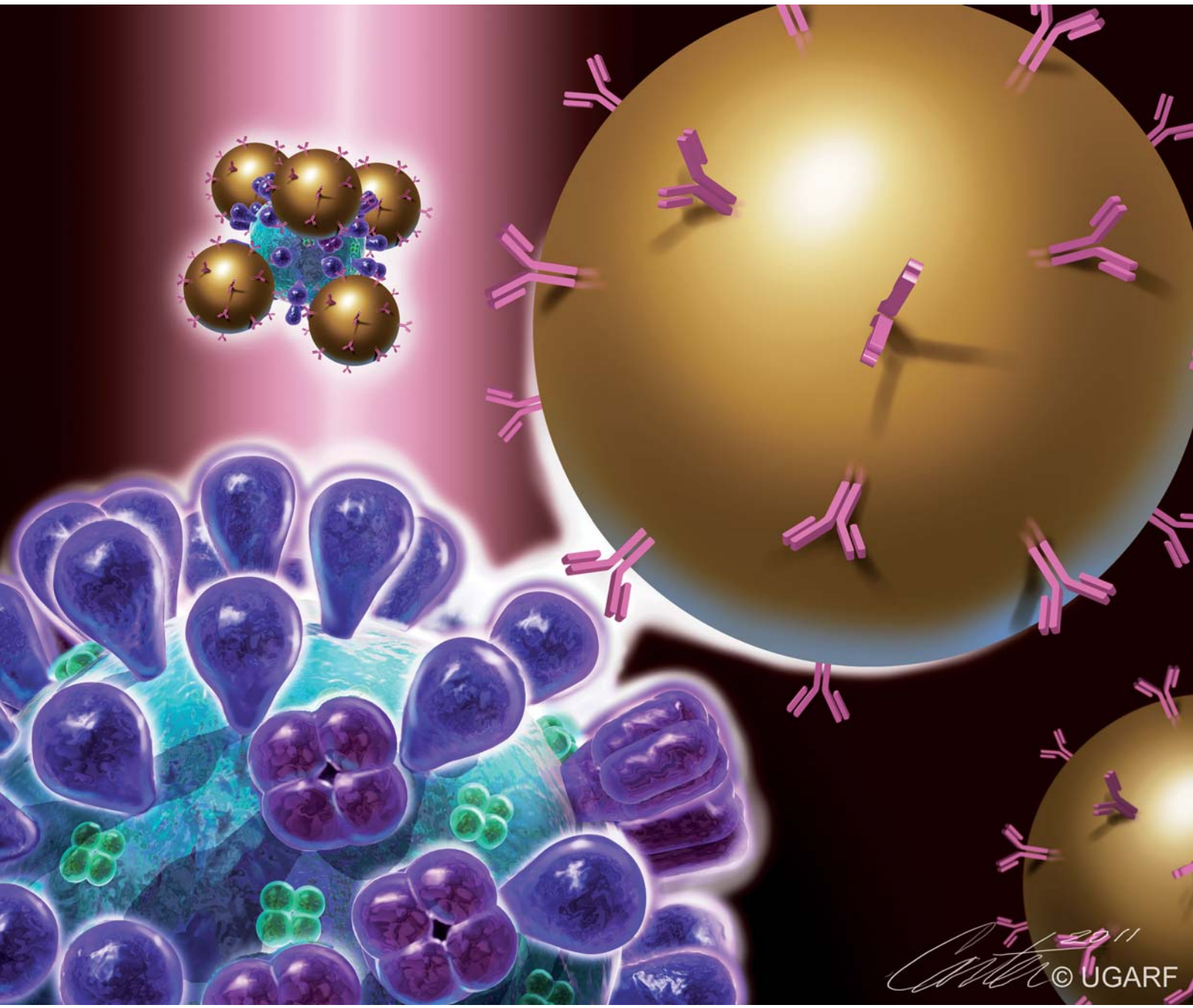

ISSN 0003-2654

RSC Publishing

PAPER

Jeremy D. Driskell *et al.*

One-step assay for detecting influenza virus using dynamic light scattering and gold nanoparticles

International Year of CHEMISTRY 2011

0003-2654(2011)136:15;1-7

Analyst

Dynamic Article Links

Cite this: *Analyst*, 2011, **136**, 3083

www.rsc.org/analyst

PAPER

One-step assay for detecting influenza virus using dynamic light scattering and gold nanoparticles†

Jeremy D. Driskell,* Cheryl A. Jones, S. Mark Tompkins and Ralph A. Tripp

Received 12th April 2011, Accepted 28th May 2011
DOI: 10.1039/c1an15303j

Herein we detail the development of a simple, rapid, and sensitive method for quantitative detection of influenza A virus using dynamic light scattering (DLS) and gold nanoparticle (AuNP) labels. Influenza-specific antibodies are conjugated to AuNPs, and aggregation of the AuNP probes is induced upon addition of the target virus. DLS is used to measure the extent of aggregation and the mean hydrodynamic diameter is correlated to virus concentration. The effects of nanoparticle concentration and size on the analytical performance of the assay were systematically investigated. It was determined that decreasing the AuNP probe concentration improves the detection limit while the effect of changing the AuNP size is minimal. Optimization of the assay provided a detection limit of <100 $TCID_{50}$/mL which is 1–2 orders of magnitude improved over commercial diagnostic kits without increasing the assay time or complexity. Additionally, this assay was demonstrated to perform equivalently for influenza virus prepared in different biological matrices.

Introduction

Influenza virus infection can cause a range of clinical symptoms resulting in at least 200,000 hospitalizations and an estimated 36,000 deaths in the United States annually.[1–3] The presentation of diverse clinical symptoms can make diagnosis difficult. Definitive diagnosis of influenza typically relies on virus isolation, antigen detection, serological response, or PCR, and each of these methods is generally time- or cost-prohibitive, thus, they are not often appropriate for clinical diagnosis. This situation is not unique to influenza, and often it is difficult, yet imperative to definitively diagnosis the causative agent in other infections as well.

Commercial immunochromatographic assays, often referred to as rapid influenza or dipstick tests, are the only available for point-of-care (POC) test that can facilitate influenza treatment. Lateral flow assays may be performed rapidly (15–30 min) and offer tremendous advantages with respect to cost, portability, shelf-life, and simplicity. However, the poor detection limits afforded by lateral flow assays result in low diagnostic sensitivity and may preclude early diagnosis due to low levels of antigen available for detection. For example, commercial lateral flow assays for influenza only provide 50–70% diagnostic sensitivity and 90–95% specificity with respect to culture-based diagnosis.[4] Moreover, these rapid antigen assays are unable to quantify viral load. Improved diagnostic sensitivity can be achieved using RT-PCR for influenza diagnosis. RT-PCR can detect as few as 100 copies/μL of viral RNA and an FDA approved kit (ProFlu+, Prodesse) is commercially available. However, RT-PCR requires a minimum of 4 h, multiple steps, specially trained personnel, and expensive reagents. Thus, RT-PCR diagnostics are limited to diagnostic laboratories and not implemented at point-of-care. It is important to note that fully automated, all-in-one RT-PCR platforms requiring only 30–45 min have been developed, but not yet received FDA approval.[5] Moreover, inherent to PCR-based approaches, these automated platforms remain to be cost-prohibitive for routine diagnostics and inhibitors present in clinical samples can prevent nucleic acid amplification to cause false negative results. It is clear that the current array of respiratory virus detection schemes is inadequate, and that the development of a rapid, sensitive, and low-cost POC diagnostic test for respiratory viruses is essential for minimizing the substantial disease burden on human health. These needs have driven an important initiative at the interface of analytical and biological sciences to develop novel methods for virus detection.

Numerous technologies are emerging to address this challenge, and those capitalizing on the unique properties of nanoparticles are some of the most promising.[6] Recent efforts employing nanoparticles for improved analysis of pathogens or pathogen-specific genes include approaches based on surface-enhanced

University of Georgia, Department of Infectious Diseases and Nanoscale Science and Engineering Center, Athens, GA, 30602, USA. E-mail: jdriskel@uga.edu; Fax: +1 706-583-0176; Tel: +1 706-542-2205

† Electronic supplementary information (ESI) available: Additional experimental details and discussions regarding antibody characterization and AuNP probe preparation are provided as ESI. Supplementary figures include: optimization of antibody-AuNP modification (Figs. S-1 and S-2), ELISA results (Fig. S-3), DLS particle size distributions (Figs. S-4 and S-5), additional TEM images (Figs. S-6 and S-7), LOD analysis and linear plots of DLS data (Figs. S-8, S-9, and S-10) and assay reproducibility (Fig. S-11). See DOI: 10.1039/c1an15303j

Raman scattering,[7–9] inductively coupled plasma mass spectrometry,[10] and piezoelectric biosensors.[11] The most extensively explored NP-based assays are colorimetric assays that capitalize on the distance dependent optical properties of AuNPs.[12,13] AuNP colorimetric assays have been developed for DNA,[14,15] protein,[16] and cells[17] and have addressed the need for simplicity, *e.g.*, single-step; however, this type of assay does not provide the requisite low level of detection, nor is it amenable to analysis of colored samples.

Recently, the highly efficient light scattering properties of gold nanoparticles have been exploited in the development of biomolecular assays in an effort to overcome the limitations of colorimetric assays.[18,19] Light scattering-based assays provided much better detection limits, *e.g.*, four orders of magnitude, than UV-visible spectrophotometric-based methods when directly compared in two independent studies.[15,20] One recently developed technique relies on the dynamic light scattering (DLS) of AuNPs to monitor the size of nanoparticle aggregates rather than a color change.[21–23] This approach to detection has been explored for the detection of DNA[21] and proteins,[22,23] and potentially offers several advantages such as the speed and simplicity of lateral flow and homogeneous assays and the low level detection limits and quantitation of a heterogeneous light scattering assay. While promising in theory, in practice, the technique provided a rather modest dynamic range and limit of detection, particularly for protein analysis.[23]

We hypothesized that the DLS technique is better suited for detecting larger targets with multiple epitopes, such as viruses, and addressed this in the present study. The principles of the assay are illustrated in Fig. 1, and the effect of analyzing a small, *e.g.*, protein or DNA, *versus* a large, *e.g.*, virus, analyte is illustrated. Briefly, AuNPs are modified with a molecular recognition element selective for a target analyte. Addition of the analyte to the AuNP probes induces crosslinking of the probes and without separation of the excess probes the mean AuNP probe/aggregate size is determined *via* DLS. At low analyte concentrations AuNP probes are in excess of the analyte and for small target molecules, *e.g.*, proteins and DNA, each molecule induces the formation of a AuNP dimer (Fig. 1A). In contrast, large analytes such as a virus can bind many AuNPs; thus, each target molecule induces the formation of a AuNP cluster consisting of several AuNP probes surrounding the virus (Fig. 1A). This difference in binding stoichiometry should result in lower detection limits and larger dynamic ranges for viral targets compared to smaller targets for three main reasons. First, as the AuNP:analyte binding ratio increases the relative number of excess single AuNP probes decreases, thereby increasing the mean hydrodynamic diameter as measured *via* DLS. Second, the increase in size from the AuNP probe to AuNP cluster for the virus is much greater than that of the AuNP probe to AuNP dimer for small targets and therefore more readily resolved as an increase in size. Third, light scattering intensity is proportional to the sixth power of diameter and it is well-established that a DLS size measurement is biased toward larger particles. As a result DLS is much more sensitive to the AuNP clusters relative to the AuNP dimmers or single AuNP probes. Similarly, the physical size and number of binding sites on the target also have implications for the assay at high analyte concentrations that benefit larger analytes as illustrated in Fig. 1B. At high concentrations the ligands on the AuNP probe will be saturated with the analyte in which case the mean hydrodynamic diameter should be approximately equal to the diameter of the AuNP probe plus twice the diameter of the target molecule. It follows then, that a larger target molecule will result in a greater upper limit for the size.

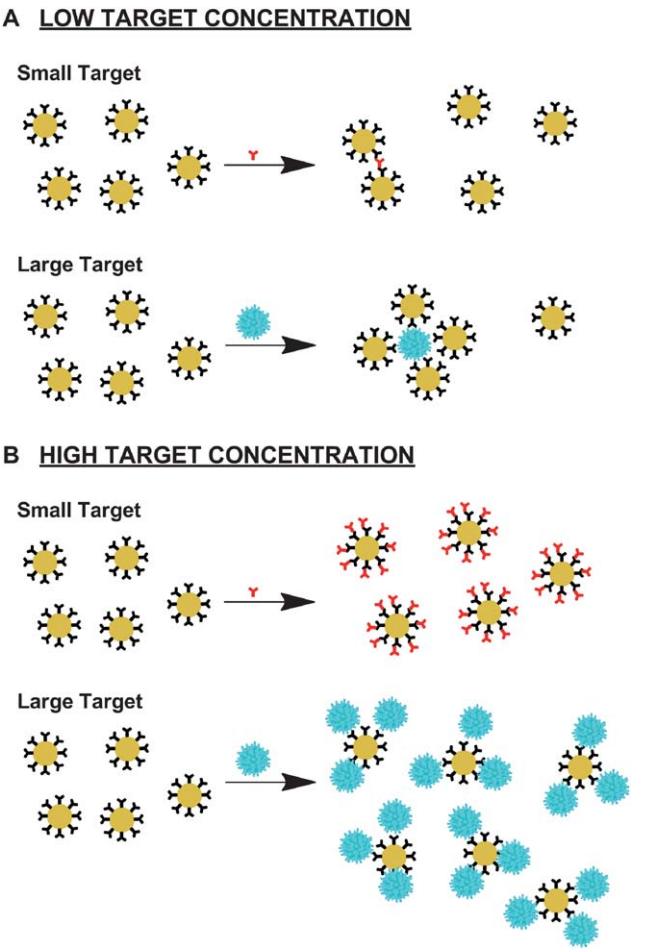

Fig. 1 Schematic comparison of analyte-induced AuNP aggregation for a small and large target analyte. The large analyte has greater impact in AuNP probe hydrodynamic diameter at both high and low analyte concentrations. See text for detailed discussion.

A proof-of-principle assay was developed for influenza A virus to investigate the feasibility of this approach for the detection of larger analytes such as viruses. Briefly, a monoclonal antibody specific for the PR8 strain of influenza A (A/PR/8/34; H1N1) was covalently conjugated to AuNPs. The AuNP probes were then added directly to samples containing influenza virus without any sample pretreatment and allowed to react. Influenza virus was quantified as a result of the increase in mean hydrodynamic radius of the AuNP probes/aggregates measured *via* DLS without separation of unbound AuNP probes. The following sections discuss investigations into the impact of AuNP probe size, AuNP probe concentration, and sample matrix on the analytical performance of the assay. It is important to note, that while this work focuses on influenza, the approach and scientific principles are readily adapted to any viral pathogen by incorporating the appropriate pathogen-specific antibody.

Experimental

Reagents

Gold nanoparticles [30 nm (2.0×10^{11} particles/mL), 60 nm (2.6×10^{10} particles/mL), 80 nm (1.1×10^{10} particles/mL)] were purchased from Ted Pella, Inc (Redding, CA). Phosphate buffered saline (PBS) was purchased from Thermo Scientific (Logan, UT). Bovine serum albumin (BSA) was obtained from Sigma (St. Louis, MO). 3,3′-Dithobis(sulfosuccinimidyl propionate) (DTSSP) was purchased from ProChem, Inc (Rockford, IL). Mouse monoclonal antibody (NR-4542, clone IC5-4F8) specific to native HA from influenza virus A/Puerto Rico/8/34 (H1N1) was obtained from BEI Resources. The antibody was purified from hybridoma supernatant *via* protein G affinity chromatography and provided at a concentration of 1 mg mL^{-1} in PBS (pH 7.4).

Viruses

Human influenza A virus strains PR/8/34 (PR8; H1N1) and A/New Caledonia/20/99 (H1N1), and swine influenza A strain MN/02719 (H3N2) were grown in 10-day old embryonated chicken eggs for 48 h at 37 °C. Eggs were obtained from a flock of specific-pathogen-free leghorn chickens (Merial Select, Gainesville, GA). Allantoic fluid from infected eggs was then collected and pooled for each strain, aliquoted, and stored at −80 °C. The 50% tissue culture infectious dose ($TCID_{50}$) of the stock viruses were determined by the Reed and Meunch method.[24] Viral titers for stocks of PR/8/34, New Caledonia, and MN/02719 were 1.9×10^6, 1.8×10^7, and 3.2×10^7 $TCID_{50}$/mL, respectively.

PR8 virus was also propagated in MDCK cells to investigate the influence of sample matrix on the assay performance. Influenza A PR/8/34 stock was diluted to a multiplicity of infection of 0.1 using infection media (MEM, 1 μM L-glutamine, 1 μg mL^{-1} TPCK-trypsin). The diluted virus (5 mL) was added to a T75 cm^2 cell culture flask containing a monolayer of MDCK cells (80–100% confluency). The culture was incubated for 48 to 72 h at 37 °C with 5% CO_2 to allow for viral replication. The supernatant was then collected, aliquoted, and stored at −80 °C. The viral titer was determined to be 1.0×10^5 $TCID_{50}$/mL as described above.

Preparation and characterization of antibody-modified AuNPs

Conjugation of AuNPs with mAb clone IC5-4F8 was adapted from a previously reported procedure[7] using DTSSP as a bi-functional cross linker. DTSSP covalently links the antibody to AuNP thereby improving the integrity of the reagent by reducing antibody desorption.[25] This is important because free antibody released from the AuNP would compete with AuNP-conjugated antibody for influenza binding sites and result in decreased assay performance. Further details can be found in Electronic Supplementary Information (ESI†). Visual assessment of AuNP color and UV-visible spectrophotometry (Beckman Coulter DU800, Brea, CA) were used to detect AuNP flocculation and establish effective coupling of the mAb to the AuNP (Figs. S-1 and S-2, ESI†).[7,26]

Immunoassay protocol

Four-fold serial dilutions of virus stocks were prepared using PBS as the diluent. A total of 90 μL of virus dilutions was added per well of a 96-well round-bottom microtiter plate (Corning, Corning, NY). Uninfected allantoic fluid and PBS served as negative control samples. The mAb-AuNP reagent (10 μL), as detailed above, was added to each well and allowed to incubate with the sample for 30 min at room temperature with gentle agitation on a plate shaker (500 rpm; IKA Works, Inc., Wilmington, NC). The AuNP reagent/sample mixture was then transferred to a 70 μL small volume disposable cuvette (Brand, Exxex, CT) for DLS analysis.

DLS measurement

A Malvern Zetasizer Nano ZS DLS system (Malvern Instruments Ltd., Worcestershire, UK) was used to conduct all DLS measurements. The DLS system is equipped with a 633 nm He–Ne laser and an avalanche photodiode detector configured to collect backscattered light at 173°. The sample was held at 25 °C by a temperature controlled sample holder and allowed to equilibrate for 60 s prior to analysis. Each size measurement was determined from 10 runs, 10 s each. Each sample was analyzed in triplicate to calculate an average and standard deviation. All DLS data were collected and analyzed using Malvern Zetasizer 6.12 software. All reported mean particle hydrodynamic diameters (D_H) are calculated from intensity based particle size distributions.

TEM analysis

Binding of whole influenza A viruses and mAb-AuNP conjugates was confirmed *via* transmission electron microscopy using a modified negative staining technique.[27] A formvar-carbon coated 400-mesh copper grid was floated on a 40-μL drop of AuNP reagent/sample mixture for 30 min at room temperature. The grid was removed and excess sample was removed with filter paper. The grid was then floated on a 40-μL drop of 0.7% glutaraldehyde for 5 min to fix the sample. After removing excess fixative, the sample was negatively stained by floating the grid on 2% aqueous phosphotungstic acid at pH 7.0 for 30 s. The stain was removed from the grid and the sample was allowed to dry overnight prior to imaging *via* TEM.

Results and discussion

Antibody reactivity

The appropriate choice of an antibody is dependent upon its intended use or assay type. As illustrated in Fig. 1, the antibody used in this assay must bind whole intact virus. Moreover, we sought to select an antibody that binds specifically to a single influenza virus strain to highlight the potential specificity of this DLS assay. Monoclonal antibody (mAb) clone IC5-4F8 was previously reported to bind the hemagglutinin (HA) of intact influenza A/Puerto Rico/8/34 (H1N1; PR8),[28] and showed limited to no cross-reactivity to other H1N1 or H3N2 influenza A viruses. We performed both ELISA and microneutralization assays to confirm these properties of mAb clone IC5-4F8 as a method of screening the antibody prior to development of the DLS assay (Fig. S-3, ESI†). Collectively, the ELISA and microneutralizaiton assays provide supportive evidence for mAb clone IC5-4F8 binding to intact PR8 virus in solution.

AuNP-antibody conjugation

UV-visible extinction spectrophotometry and DLS size analysis were used to characterize mAb-labeled AuNP and compare to the as-received unconjugated AuNP. The surface plasmon resonance band red-shifted from 534 nm for 60-nm unconjugated AuNP to 538 nm for the mAb-AuNP conjugate. This small shift in λ_{max} is expected and is the result of a change in the local refractive index around the AuNP due to the antibody. The yield of mAb-AuNP conjugates varied for each preparation (40–75%) based on estimates calculated using the extinction magnitude at λ_{max}. The loss of AuNP during preparation of the conjugate and range of yields is due to experimental variability associated with multiple centrifugation/decantation/resuspension cycles. The average D_H for the AuNP increased from 65.2 nm to 103.6 nm as determined *via* DLS after conjugation with mAb clone IC5-4F8 while the peak width, *e.g.*, size distribution, did not change. The slight overestimate in the DLS measured size relative to the TEM determined size of 60 nm for the unconjugated AuNPs is due to the fact that DLS measures the hydrodynamic diameter and the unconjugated AuNP is suspended in water with few ions; consequently the double layer is large. Upon conjugation of the antibody to the AuNP, the apparent increase in particle size is 38.4 nm while the expected increase should be ~15–20 nm assuming a full layer of antibody coating the AuNP and a hydrodynamic diameter of 7–10 nm for each IgG antibody. However, the observed increase in D_H is consistent with the range (15–60 nm) reported by Jans *et al.* in which the DLS measured size increase resulting from AuNP-antibody conjugation was determined to be dependent upon conjugation time and antibody concentration.[20]

DLS assay

To demonstrate the practicability of the DLS assay and to establish that mAb clone IC5-4F8 maintains its activity toward PR8 upon conjugation to AuNP, the size of mAb-AuNP reagent (10 μL, 2.6×10^{10} NP/mL) before and after mixing with PR8 (90 μL, 1.2×10^5 $TCID_{50}$/mL) was measured *via* DLS (Fig. S-4, ESI†). The intensity-based size distribution is plotted in Fig. S-4 (ESI) and reveals an increase in the mean D_H from 103.6 nm to 390.0 nm upon the addition of PR8, indicating influenza-induced aggregation. TEM analysis corroborates PR8-induced aggregation of AuNP probes. These data confirm that sufficient antibody is appropriately oriented and retains antigen binding ability and the ability of PR8 virions to crosslink multiple AuNP probes into aggregates. Importantly, the sample was not treated or processed prior to the addition of AuNP probes and DLS analysis. AuNP is a much more efficient light scatterer than biological molecules found in biological matrices; thus, DLS is only sensitive to the AuNP probes. It is also important to note that this is a single step homogeneous assay in which virus-induced aggregates are not separated from excess, free mAb-AuNP reagent. Thus, the mean D_H recorded in this assay reflects the size of both the unbound single AuNP reagent as well as any influenza-bound aggregated AuNP reagent with the caveat that the intensity distribution is inherently biased toward larger particles/aggregates.

Dilutions of influenza virus, PR8 and New Caledonia strains, were prepared from allantoic fluid stocks. PR8 sample concentrations covered five orders of magnitude (4.8×10^5 to 7.2×10^1 $TCID_{50}$/mL) while New Caledonia sample concentrations ranged from 1.4×10^6 to 5.5×10^3 $TCID_{50}$/mL. AuNP probes (10 μL, 2.6×10^9 NP/mL) were mixed with the sample solutions or PBS, *e.g.*, negative control, for 30 min and the mean D_H was measured *via* DLS (Fig. S-5, ESI†). The DLS assay results in Fig. 2A show an increase in mean D_H with an increase in PR8 up to a concentration of 3.0×10^4 $TCID_{50}$/mL. Greater concentrations of PR8 led to a decrease in D_H. This decrease in signal, *i.e.*, size, at high concentration is a commonly observed phenomenon known as the prozone, hook effect, or rollover effect[29,30] and was previously reported for a DLS assay for mouse IgG.[23] The peak signal is referred to as 'hook point' and at concentrations above the hook point the relative number of virions is in excess of the binding sites on the AuNP probes resulting in reduced crosslinking. At some sufficiently high analyte concentration complete loading of AuNP probes with individual virions will occur and the D_H will reach a constant D_H value equal to the diameter of AuNP plus two times the diameter of the analyte as illustrated in Fig. 1. Due to the large size of the viral target in comparison to the protein target[23] the signal decay above the hook point is less prominent.

In contrast to the DLS assay for protein,[23] the shape of the response curve is sigmoidal and the particle size increase was significant even at low concentrations between 2.9×10^1 and 3.0×10^4. This observation is due to the fact that at low concentrations, in the absence of extensive influenza-induced aggregation, a single viral particle can bind multiple AuNP significantly increasing the effective diameter of the bound AuNP probe. In comparison to low levels of a small target such as a protein or DNA, at most, a dimer of AuNPs is formed which has minimal effect of the D_H even for the bound AuNP dimer (Fig. 1).

To validate our understanding of the assay and resulting curve shape, TEM micrographs were collected for the sample-probe mixtures at three regions of the calibration curve: below, equal to, and above the hook point. Representative TEM images of the three regions are displayed in Fig. 2. At low concentrations of influenza virus, the viral particle is completely encapsulated by AuNP probes as is suggested in Fig. 2B. AuNP clusters of 6–8 AuNPs were prevalent at this concentration suggesting that a central virion is consistently forming the core of these clusters; however, it was not possible to get direct visualization of the central virus. Fig. 2C illustrates the extensive crosslinking between influenza viruses and AuNP probes to form large aggregates. At high viral loads each probe binds many virions as is evident in Fig. 2D, thereby significantly increasing the effective size of each of the bound probes relative to their unbound state. Additional TEM images are provided in Figs. S-6 and S-7 (ESI) as further support for the interpretation of the DLS calibration curve shape.

To fully evaluate the limit of detection, the DLS data for low concentrations of virus were plotted on a linear scale and best-fit to a linear function (Fig. S-8, ESI†). The detection limit for the assay was 8.6×10^1 $TCID_{50}$/mL and was calculated as the concentration of PR8 which provides a signal that is greater than the signal for the PBS blank sample (103.0 ± 2.5 nm) plus three times its standard deviation. This is orders of magnitude improved over the detection limits by FDA-approved commercial influenza test kits which are reported to range from 2.5×10^3

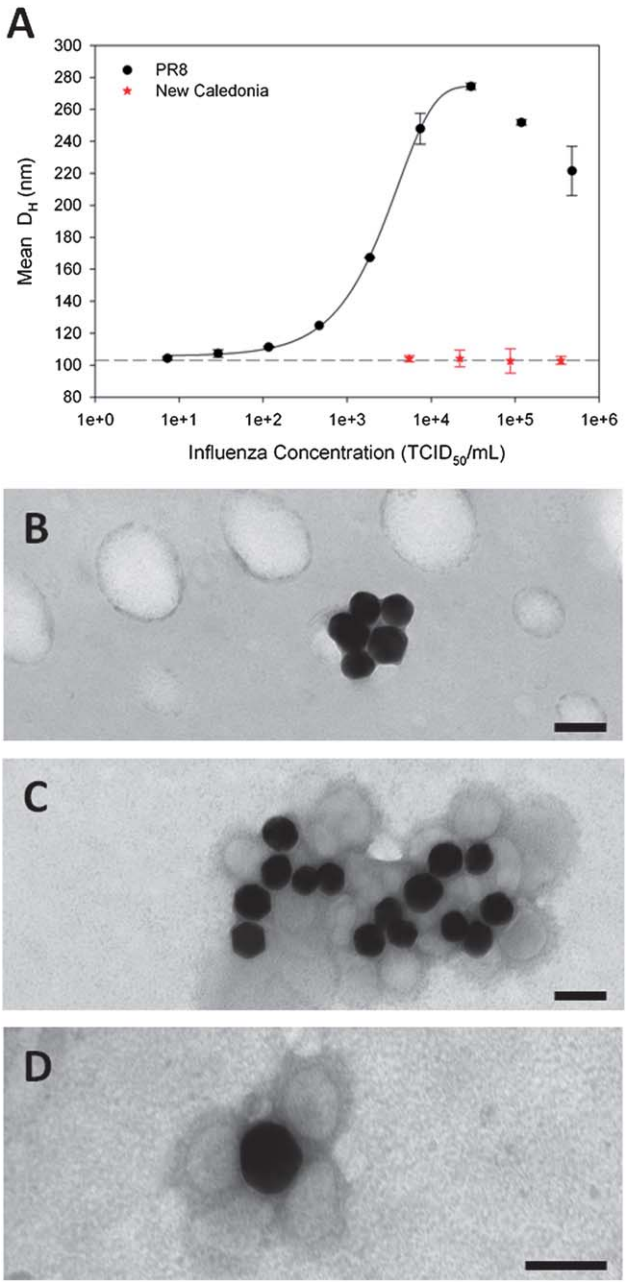

Fig. 2 DLS calibration curve for influenza virus assay and corresponding TEM micrographshs. (A) Mean hydrodynamic diameter (D_H) of AuNP and AuNP aggregates measured *via* DLS as a function of influenza virus concentration for two strains: PR8 and New Caledonia. The horizontal dashed line represents the measured mean D_H for the AuNP reagent plus negative control sample, *i.e.*, PBS. Representative TEM micrographs for the reaction of AuNP probes with PR8 at viral concentrations of (B) 4.9×10^5 $TCID_{50}$/mL, (C) 3.0×10^4 TCID50/mL, and (D) 4.6×10^2 TCID50/mL. The scale bars represent 100 nm.

to 1.0×10^4 TCID50/mL.[31] In addition, it should be noted that the commercial rapid chromatographic immunoassays do not provide any quantitative information.

The AuNP probe did not aggregate upon addition to the PBS negative control (Fig. 2A, dashed line), nor did the AuNP probe aggregate when mixed with several concentrations of influenza A New Caledonia (Fig. 2A, red triangles). These results demonstrate the high degree of specificity for the PR8 strain imparted by mAb clone IC5-4F8, and is in accordance with the ELISA results (Fig. S-3, ESI†).

Effect of AuNP concentration

It is expected that AuNP probe concentration will have a marked effect on the DLS assay. Fig. 1 suggests that a decrease in AuNP probe concentration for a given PR8 concentration will result in a greater percentage of probes in an aggregated cluster with fewer single probes remaining in solution. In effect, this would result in an increased mean D_H as measured by DLS to yield a more sensitive assay. This premise was investigated by conducting the DLS assay for PR8 using four concentrations of AuNP probe and comparing the dynamic range and detection limit for each assay.

Fig. 3 shows the response curves of the DLS assays using 60 nm AuNP probes at concentrations of 10x AuNP (2.6×10^{11} NP/mL), 1x AuNP (2.6×10^{10} NP/mL), 0.1x AuNP (2.6×10^9 NP/mL), and 0.01x AuNP (2.6×10^8 NP/mL). The data support the hypothesis that a decrease in AuNP probe concentration results in a larger mean size, but only for concentrations below the hook point. Moreover, the hook point occurs at a lower PR8 concentration with decreasing AuNP concentrations, as expected, since fewer mAb binding sites are available leading to saturation at lower PR8 levels. The dynamic range is shifted to lower levels for lower AuNP probe concentrations, and the detection limits followed a similar trend with values of 1.6×10^3, 4.8×10^2, 8.6×10^1, and 2.5×10^2 TCID50/mL, respectively, for 10x, 1x, 0.1x, and 0.01x AuNP probe (Fig. S-9, ESI†). The best detection limit was not achieved with the lowest probe concentration, *i.e.*, 0.01x AuNP, as expected, due to an increase in the mean size measurement error for 0.01x AuNP probe as reflected by the error bars in Fig. 3 resulting in a worse detection limit compared to the 0.1x AuNP probe assay. It is worth noting that at 0.01x AuNP, the scattering signal for the AuNP is only slightly above the intensity of the scattering signal provided by the

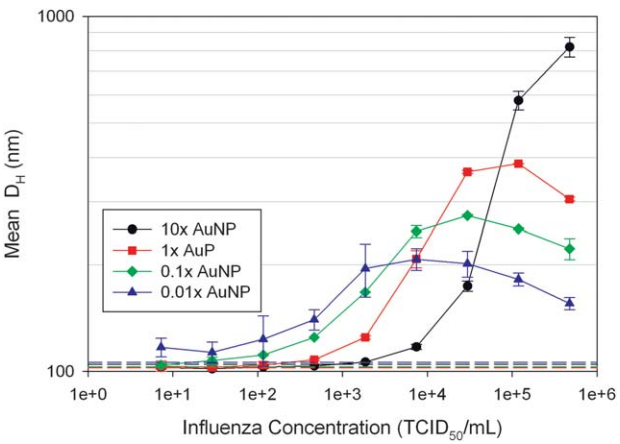

Fig. 3 Effect of AuNP probe concentration on the DLS assay performance for influenza virus. Dilutions of influenza A PR8 or PBS were reacted with 10x AuNP (2.6×10^{11} NP/mL), 1x AuNP (2.6×10^{10} NP/mL), 0.1x AuNP (2.6×10^9 NP/mL), and 0.01x AuNP (2.6×10^8 NP/mL). The horizontal dashed lines represent the measured mean D_H for the AuNP reagent plus PBS negative control samples.

biological molecules in the background sample matrix. These assays suggest that a minimum concentration of AuNP probe is desirable to achieve the lowest detection limit; however the biological matrix must be considered such that scattering from the matrix is less than that of the AuNP probes.

Also apparent in the response curves plotted in Fig. 3 is the increase in aggregate size at the hook point with an increase in AuNP probe concentration. This finding is intuitive given that more AuNP probes allows for more extensive aggregation. Moreover, Storhoff *et al.*[32] have demonstrated that AuNP aggregate size is kinetically controlled with faster reactions yielding larger aggregates. Our data is consistent with that previous work, given that the aggregation rate correlates with AuNP probe concentration.

Effect of AuNP size

DLS assays for PR8 were performed using 1x (concentration as received) AuNP reagents with core diameters of 30, 60, and 80 nm. The response curves for the assays are given in Fig. 4. In contrast to the concentrations studies above, under these experimental conditions, AuNP probe size is found to have minimal effect on the assay performance. The D_H approaches limiting values of 68.2 nm, 98.2 nm, and 121.5 nm, respectively, for the 30 nm, 60 nm, and 80 nm AuNP probes as the PR8 concentration approaches zero as expected based on the size of the gold nanoparticle that serves as the probe cores. Detection limits were calculated based on linear analysis of the low concentration samples (Fig. S-10, ESI†) and determined to be 1.6×10^2, 2.8×10^2, and 5.6×10^2 $TCID_{50}$/mL for the 30, 60, and 80 nm AuNP probes, respectively. Although the hook point is slightly shifted to higher concentrations for the 30 nm AuNP probe, the hook point is similar for each of these assays. These results appear to contradict those of the concentration studies presented in the previous section given that the AuNP probe concentrations significantly differ. Based on the previous findings, one may expect the assay employing the 30 nm AuNP probe to provide the worst detection limit because it is the most concentrated by a factor of 10 to 20 compared to the 60 nm and 80 nm AuNP probes, respectively. However, it is important to consider the binding stoichiometry between the probes and the virion. Based on steric hinderance, the AuNP probe size is inversely correlated to the number bound to the virion. Consequently, at low concentrations in which the virus is fully encapsulated by the AuNP probe, more 30 nm AuNP probes bind per virus than 60 nm or 80 nm probes. As a result a greater percentage of small particles are bound to the virus leaving fewer excess probes to reduce the mean D_H. Additionally, the effective diameter of the 30 nm probe undergoes a much greater increase when complexing with the virion compared to the 60 nm or 80 nm probe which is more readily detected over single, unbound probes.

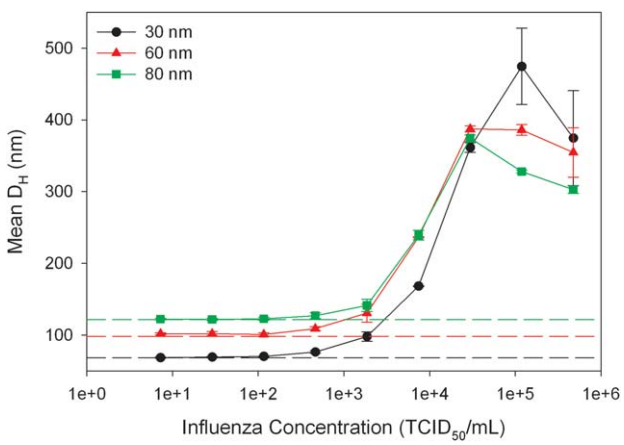

Fig. 4 Effect of AuNP probe size on the DLS assay performance for influenza virus. Dilutions of influenza A PR8 or PBS were reacted with 30 nm AuNP (2.0×10^{11} NP/mL), 60 nm AuNP (2.6×10^{10} NP/mL), or 80 nm AuNP (1.1×10^{10} NP/mL). The horizontal dashed lines represent the measured mean D_H for the AuNP reagent plus PBS negative control samples.

Reproducibility and AuNP probe stability

The reproducibility of a diagnostic test must be established to fully demonstrate the utility of the assay. The reproducibility of the assay as well as the stability of the AuNP probe over time was investigated. Numerous assays were performed over several months during the development and optimization of this technique. We observed that the calibration curves were similar in shape for each assay, including peak D_H at the hook point, yet the dynamic range could slightly vary from assay to assay (Fig. S-11, ESI†). The loss of AuNP probes as a result of multiple centrifugation and resuspension steps varied between preparations and is likely the cause of the deviation in the dynamic range based on the findings presented above, *i.e.*, Effect of AuNP Probe Concentration. While probe concentration was found to be critical for obtaining reproducible results, this can be easily controlled by monitoring the AuNP probe concentration *via* UV-visible spectrophotometry and appropriate dilution. Alternatively, a large batch of probe could be prepared and repeatedly used provided that the probes are stable over time.

To investigate the probe stability and assay reproducibility for a constant probe concentration, a single batch of 60 nm AuNP probe was prepared on day 1. This batch of AuNP probes was used to perform three assays for PR8 on three consecutive days, storing the probes at 4 °C between uses. The results for the assays are shown in Fig. 5. The calibration curves demonstrate the high level of reproducibility among assays for a constant AuNP probe concentration. Moreover, no degradation in assay performance is observed, establishing the stability of the AuNP-antibody conjugate. These data suggest that once the assay is calibrated for one preparation of AuNP probe, the curve is valid for a minimum of one week.

Matrix effect

It is critical that a bioanalytical assay is compatible with multiple sample types or background matrices to maximize its utility. For example, viral propagation methods vary with influenza being propagated in embryonated chicken eggs and in mammalian cell culture. When considering clinical samples the background matrix depends on the collection method, *e.g.*, sputum, nasal wash, *etc.* Moreover, the clinical background for a single sample type will vary from subject-to-subject. Thus, it is imperative that the background matrix does not affect the assay signal.

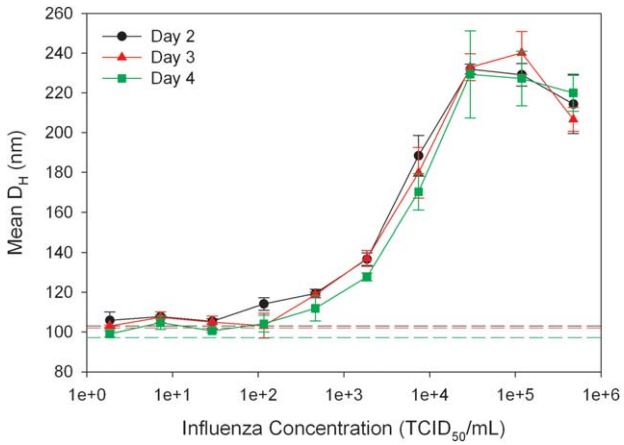

Fig. 5 DLS assay for influenza virus performed on consecutive days to investigate the stability of AuNP probes. Dilutions of influenza A PR8 or PBS were independently prepared on consecutive days and reacted with 60 nm AuNP probes stored at 4 °C between uses. The horizontal dashed lines represent the measured mean D_H for the AuNP reagent plus PBS negative control samples.

Biomolecules are intrinsically weak light scattering molecules whereas AuNPs are extremely efficient light scatterers. Thus, even in the relatively high concentrations of biomolecules found in biological matrices, scattered signal from AuNP overwhelms that of the background, and it is anticipated that this difference in light scattering efficiency will allow the detection of AuNP probes *via* DLS in most biological matrices. To test the effect of sample matrix on the DLS assay, PR8 was grown in embryonated chicken eggs and MDCK cells. After 48 h, the virus was harvested in allantoic fluid or the supernatant of lysed cells in cell culture medium. PR8 is an egg-adapted strain and replicates more efficiently in eggs than cell cultures. Thus, the viral titers for the two samples were 1.9×10^6 and 1.0×10^5 $TCID_{50}$/mL, respectively, for the egg and cell prepared stocks. Four-fold dilutions of each of the stocks were prepared and assayed.

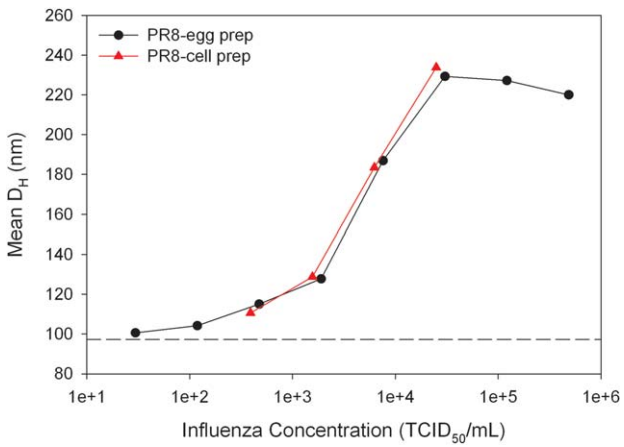

Fig. 6 DLS assay for influenza virus isolated in allantoic fluid and MDCK cell supernatant to investigate the effect of sample matrix. Dilutions of influenza A PR8 or PBS were reacted with 60 nm AuNP probes. The horizontal dashed lines represent the measured mean D_H for the AuNP reagent plus PBS negative control samples.

Calibration curves for each of the sample types were statistically equivalent (Fig. 6). These results confirm that the DLS readout of AuNP probe aggregation is independent of the sample matrix.

Conclusions

In this study, we demonstrate simple, rapid, sensitive, and quantitative detection of influenza A/Puerto Rico/8/34 in a single-step homogeneous format using AuNP probes and DLS for readout. This assay offers a significant improvement with respect to detection limits compared to lateral flow and colorimetric-based AuNP aggregation assays. Moreover, this assay provides valuable quantitative information and is compatible with colored samples. This work not only extends the application of a DLS-based assay to the detection of viruses, it elucidates inherent properties of this approach which make it better suited for virus detection in comparison to smaller analyte targets such as DNA and proteins. This assay could be easily implemented in most laboratories for a wide variety of pathogens. Unconjugated AuNP and antibodies are commercially available and cost-effective. Previous work suggests that, once prepared, the AuNP conjugate can be stored up to a year without loss in activity;[33] thus samples can be immediately analyzed in less than 30 min. Moreover, while the initial expense of a DLS instrument is already reasonable for diagnostic laboratories, as the price is driven lower by expanding applications of DLS and manufacturer competition, the potential for wide spread acceptance and implementation will be increasingly feasible. Perhaps the most attractive aspect of this assay is the versatility of the approach. The assay specificity with respect to viral subtype or strain can be adjusted by the selected antibody. Moreover, this assay format is readily adapted to any viral target for which an antibody is available.

Acknowledgements

This work was supported by a UGA Faculty Research Grant, DoD-ARL contract W911NF-11-2-0010, and NIAID CEIRS contract HHSN266200700006C. The following reagent was obtained through the NIH Biodefense and Emerging Infections Research Resources Repository, NIAID, NIH: Monoclonal Anti-Influenza A Virus HA, Clone IC5-4F8, NR-4542. The authors would like to thank Scott Johnson and Spencer Poore for assistance with the ELISA experiments and Jon Gabbard for guidance with the microneutralization assays.

Notes and references

1 W. W. Thompson, D. K. Shay, E. Weintraub, I. Brammer, C. B. Bridges, N. J. Cox and K. Fukuda, *JAMA, J. Am. Med. Assoc.*, 2004, **292**, 1333–1340.
2 W. W. Thompson, D. K. Shay, E. Weintraub, L. Brammer, N. Cox, L. J. Anderson and K. Fukuda, *JAMA, J. Am. Med. Assoc.*, 2003, **289**, 179–186.
3 WHO, World Health Organization, 2010.
4 A. Gordon, E. Videa, S. Saborio, R. Lopez, G. Kuan, A. Balmaseda and E. Harris, *Plos One*, 2010, **5**, Article No.: e10364.
5 EnigmaDiagnostics, 2011.
6 N. L. Rosi and C. A. Mirkin, *Chem. Rev.*, 2005, **105**, 1547–1562.
7 J. D. Driskell, K. M. Kwarta, R. J. Lipert, M. D. Porter, J. D. Neill and J. F. Ridpath, *Anal. Chem.*, 2005, **77**, 6147–6154.
8 J. D. Driskell, Y. Zhu, C. D. Kirkwood, Y. P. Zhao, R. A. Dluhy and R. A. Tripp, *PLoS One*, 2010, **5**.

9 I. S. Patel, W. R. Premasiri, D. T. Moir and L. D. Ziegler, *J. Raman Spectrosc.*, 2008, **39**, 1660–1672.
10 F. Li, Q. Zhao, C. A. Wang, X. F. Lu, X. F. Li and X. C. Le, *Anal. Chem.*, 2010, **82**, 3399–3403.
11 S. H. Chen, V. C. H. Wu, Y. C. Chuang and C. S. Lin, *J. Microbiol. Methods*, 2008, **73**, 7–17.
12 P. Baptista, E. Pereira, P. Eaton, G. Doria, A. Miranda, I. Gomes, P. Quaresma and R. Franco, *Anal. Bioanal. Chem.*, 2008, **391**, 943–950.
13 W. Zhao, M. A. Brook and Y. F. Li, *ChemBioChem*, 2008, **9**, 2363–2371.
14 H. X. Li and L. Rothberg, *Proc. Natl. Acad. Sci. U. S. A.*, 2004, **101**, 14036–14039.
15 J. J. Storhoff, A. D. Lucas, V. Garimella, Y. P. Bao and U. R. Muller, *Nat. Biotechnol.*, 2004, **22**, 883–887.
16 C. S. Tsai, T. B. Yu and C. T. Chen, *Chem. Commun.*, 2005, 4273–4275.
17 C. D. Medley, J. E. Smith, Z. Tang, Y. Wu, S. Bamrungsap and W. H. Tan, *Anal. Chem.*, 2008, **80**, 1067–1072.
18 J. Ling, C. Z. Huang, Y. F. Li, L. Zhang, L. Q. Chen and S. J. Zhen, *TrAC, Trends Anal. Chem.*, 2009, **28**, 447–453.
19 J. Yguerabide and E. E. Yguerabide, *Anal. Biochem.*, 1998, **262**, 157–176.
20 H. Jans, X. Liu, L. Austin, G. Maes and Q. Huo, *Anal. Chem.*, 2009, **81**, 9425–9432.
21 Q. Dai, X. Liu, J. Coutts, L. Austin and Q. Huo, *J. Am. Chem. Soc.*, 2008, **130**, 8138.
22 X. Liu, Q. Dai, L. Austin, J. Coutts, G. Knowles, J. H. Zou, H. Chen and Q. Huo, *J. Am. Chem. Soc.*, 2008, **130**, 2780.
23 X. Liu and Q. Huo, *J. Immunol. Methods*, 2009, **349**, 38–44.
24 L. J. Reed and H. HMuench, *Am. J. Hyg.*, 1938, **27**, 493–497.
25 J. Ni, R. J. Lipert, G. B. Dawson and M. D. Porter, *Anal. Chem.*, 1999, **71**, 4903–4908.
26 W. D. Geoghegan and G. A. Ackerman, *J. Histochem. Cytochem.*, 1977, **25**, 1187–1200.
27 M. A. Hayat and S. E. Miller, *Negative Staining*, McGraw-Hill, New York, 1990.
28 J. W. Yewdell, R. G. Webster and W. U. Gerhard, *Nature*, 1979, **279**, 246–248.
29 S. Dodig, *Biochem. Medica.*, 2009, **19**, 50–62.
30 C. Selby, *Ann. Clin. Biochem.*, 1999, **36**, 704–721.
31 E. McFarland, A. Yup, S. Joshi, S. Lovell, J. Stahler, C. Finnerty, B. Pope, J. Newman and V. Crews, in *Clinical Virology Symposium*2005.
32 J. J. Storhoff, A. A. Lazarides, R. C. Mucic, C. A. Mirkin, R. L. Letsinger and G. C. Schatz, *J. Am. Chem. Soc.*, 2000, **122**, 4640–4650.
33 J. E. Beesley, *Colloidal Gold: A New Perspective for Cytochemical Marking*, Oxford Universitiy Press, Oxford, U.K., 1989.

